Machine-learning correction of the local effects on neutron monitor and muon detector count rates at Syowa Station in the Antarctic

Ryuho Kataoka (1,2,3), Tatsuhiko Sato (4), Chihiro Kato (5), Akira Kadokura (6,1,2), Masayoshi Kozai (6), Shoko Miyake (7), Kiyoka Murase (2), Lihito Yoshida (2), and Yoshihiro Tomikawa (1,2), and Kazuoki Munakata (5)

(1) National Institute of Polar Research, Japan
(2) The Graduate University for Advanced Studies, SOKENDAI, Japan
(3) Okinawa Institute of Science Technology Graduate University, Japan
(4) Japan Atomic Energy Agency, Japan
(5) Shinshu University, Japan
(6) Polar Environment Data Science Center, Joint Support-Center for Data Science Research, Research Organization of Information and Systems, Japan
(7) National Institute of Technology (KOSEN) Ibaraki College, Japan

Abstract:
Solar modulation of galactic cosmic rays around the solar minimum in 2019-2020 looks different in the secondary neutrons and muons observed at the ground. To compare the solar modulation of primary cosmic rays in detail, we must remove the possible seasonal variations caused by the atmosphere and surrounding environment. As such surrounding environment effects, we evaluate the snow cover effect on neutron count rate and the atmospheric temperature effect on muon count rate, both simultaneously observed at Syowa Station in the Antarctic (69.01 S, 39.59 E). A machine learning technique, Echo State Network (ESN), is applied to estimate both effects hidden in the observed time series of the count rate. We show that the ESN with the input of ERA5 reanalysis data (temperature time series at 1000, 700, 500, 300, 200, 100, 70, 50, 30, 20, and 10 hPa) at the closet position can be useful for both the temperature correction for muons and snow cover correction for neutrons. The corrected muon count rate starts decreasing in late 2019, earlier than the corrected neutron count rate, which starts decreasing in early 2020, possibly indicating the rigidity-dependent solar modulation in the heliosphere.

This manuscript has been submitted for publication in *Journal of Space Weather and Space Climate*. Please note that, despite having undergone peer-review, the manuscript has yet to be formally accepted for publication. Subsequent versions of this manuscript may have slightly different content. If accepted, the final version of this manuscript will be available via a link on this webpage.

1. Introduction

Measuring galactic cosmic rays (GCR) is important and plays a unique role in diagnose the space weather and space climate. For example, the real-time data of worldwide neutron monitor network is utilized for predicting the radiation dose of aircrews during ground-level enhancement (GLE) events (Kataoka et al., 2014; Sato et al., 2018; Kataoka et al., 2018). The long-term GCR data is also used to examine the solar cycle prediction of the aircrew dose (Miyake et al., 2017). Furthermore, for transient space weather events such as coronal mass ejections (CMEs) passing through the Earth, we can also estimate the large-scale magnetic field structure of CMEs by analyzing the Global Muon Detector Network (GMDN) data (Kihara et al., 2021).

We started neutron and muon measurements at Syowa Station in the Antarctic (69.01 S, 39.59 E; the vertical cutoff rigidity is 0.4 GV) in February 2018 (Kato et al., 2021). The simultaneous observation of neutron and muon is a unique point compared to the other neutron monitors and muon detectors. The median primary rigidities for the neutron monitor and muon detector (vertical) are 16.3 GV and 53.6 GV, respectively (**Appendix A**). We estimated the median primary rigidities by integrating the response functions of secondary neutrons and muons to primary cosmic rays (Nagashima et al., 1989; Murakami et al., 1979).

During the 4-year cosmic ray observation at Syowa Station, the solar activity gradually changes across the solar minimum. **Figure 1** shows the solar-minimum part of the so-called 11-year solar modulation of GCR. The top panel shows the Sun's polar magnetic field (http://wso.stanford.edu/). The north-south average of the magnetic field strength (green dots) started decreasing in late 2019. The second panel shows the sunspot number (https://www.sidc.be/silso/), passing through the solar minimum in late 2019. The bottom panel shows the neutron monitor count rate at Oulu (https://cosmicrays.oulu.fi/), starting to decrease in early 2020.

This paper aims to report the first 4-year data of neutron count rate and muon count rate (6-hour values) at Syowa Station to contribute to discussing the energy-dependent solar modulations in the latest solar minimum. For that purpose, the atmospheric and environmental calibrations are important for muon and neutron data, as introduced in Section 2. Specifically, the temperature correction is essential for muons, while the snow cover correction is vital for neutrons (Bütikofer, 2017). Section 2.3 proposes a new method for the snow cover correction based on the analytical radiation model. In Section 3, we discuss that a machine-learning technique combined with meteorological reanalysis data can be useful for these different corrections for muons and neutrons. Finally, concluding remarks are summarized in Section 4.

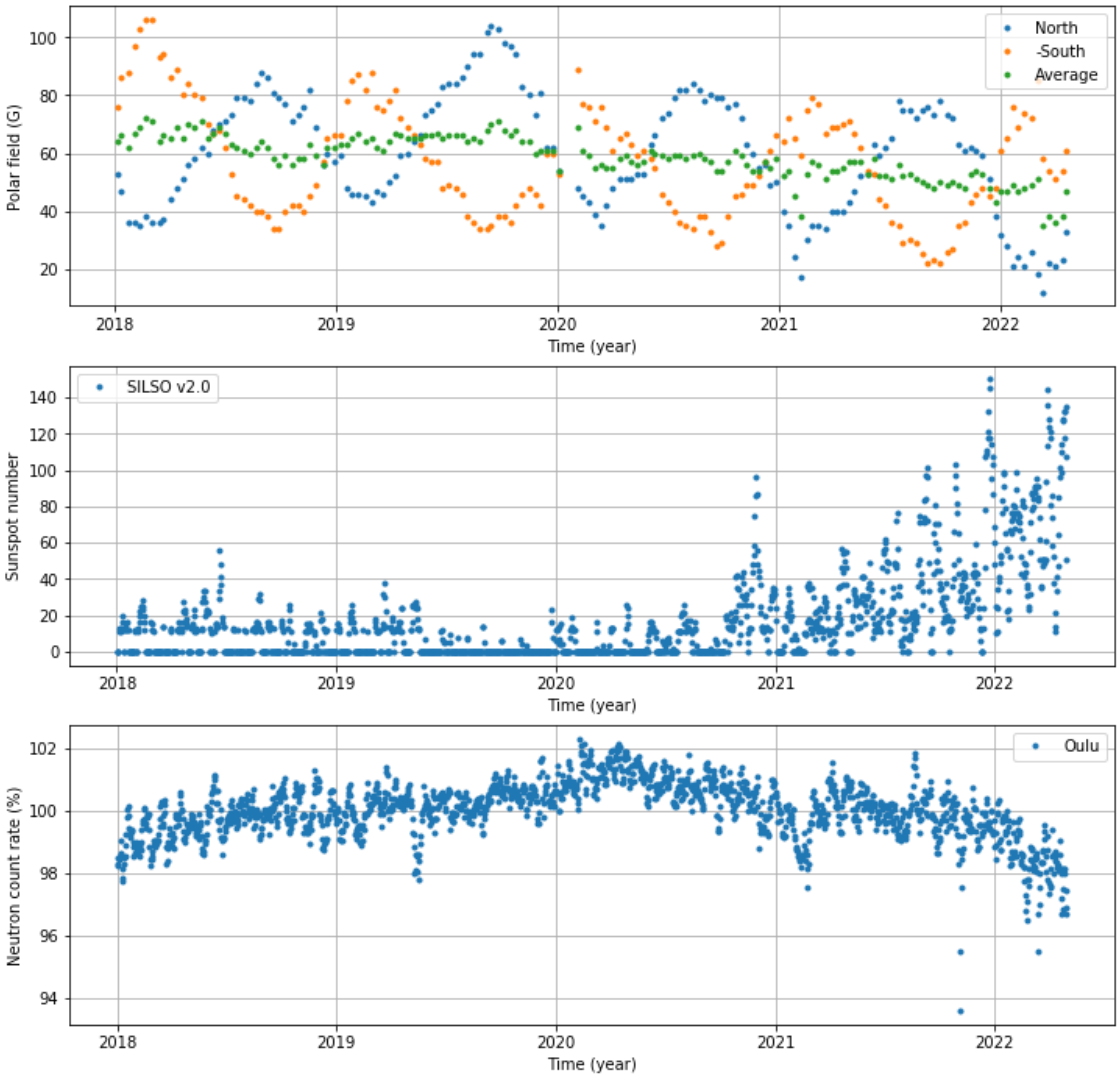

Figure 1. (a) The 10-day values of 30-day running averaged Sun's polar magnetic field, (b) daily mean sunspot number, and (c) daily mean neutron monitor count rate at Oulu, Finland. The polar magnetic field strength (green dots) started decreasing in late 2019, while the neutron count rate started decreasing in early 2020.

2. Methods of analysis

2.1. ESN for muon and neutron counting rates

The Echo State Network (ESN) is a kind of recurrent neural networks (Jaeger, 2001). The basic structure of the ESN model used in this paper is essentially the same as was used by Kataoka and Nakano (2021). Therefore, only the essential part is repeated below. The input vector **u**, reservoir state vector **x**, and output vector **y** are defined by N-points time series of n = 1,2,3…N as follows:

$$\mathbf{u}(n)=\begin{pmatrix} u_1(n) \\ \vdots \\ u_{Nu}(n) \end{pmatrix},\ \mathbf{x}(n)=\begin{pmatrix} x_1(n) \\ \vdots \\ x_{Nx}(n) \end{pmatrix},\ \mathbf{y}(n)=\begin{pmatrix} y_1(n) \\ \vdots \\ y_{Ny}(n) \end{pmatrix} \tag{1}$$

The reservoir state vector **x** consists of a large number of nodes, which are updated in time with the input vector **u** and the previous state of the nodes as follows:

$$\mathbf{x}(n+1)=f\left(W^{in}\mathbf{u}(n+1)+W\mathbf{x}(n)\right)\ \ (n=0,1,2,...), \tag{2}$$

where we use hyperbolic tangent as the function f and fix the weight matrices W^{in} and W. To make the random and sparse node connections of W, we set the number of nodes, Nx, to be 10^3, where only 10 % of the matrix elements are random values between -1.0 to 1.0, and the rest 90 % are zero. We selected the spectral radius (maximum eigenvalue) of W below unity to satisfy the echo state property that guarantees the independence of the reservoir state to the initial values (Jaeger, 2001). In this paper, we optimized the spectral radius to be 0.95 (**Appendix B**). The output vector **y** is calculated by the linear combination of the output weight matrix and the reservoir state vector as follows:

$$\mathbf{y}(n+1)=W^{out}\mathbf{x}(n+1)\ \ (n=0,1,2,...), \tag{3}$$

where W^{out} is the output weight matrix. We train only the output weight matrix by the set of T-point time series of input vectors X and desired output vectors D:

$$X=\left[\mathbf{x}(1),...,\mathbf{x}(T)\right],\ \ D=\left[\mathbf{d}(1),...,\mathbf{d}(T)\right]. \tag{4}$$

The least-squares method to minimize the difference between the outputs **y** and **d** can be represented by a standard linear regression as follows:

$$W^{out}=DX^{T}(XX^{T})^{-1}. \tag{5}$$

For the temperature data, we used ERA5 (the fifth generation European Centre for Medium-Range Weather Forecasts atmospheric reanalysis) hourly values at geographic coordinates (69 S, 40 E), sampled at 11 layers at 1000, 700, 500, 300, 200, 100, 70, 50, 30, 20, and 10 hPa (Hersbach et al., 2020; https://www.ecmwf.int/en/forecasts/dataset/ecmwf-reanalysis-v5). In the above ESN model (Kataoka and Nakano, 2021), we use temperature data as the 11-dimensional input vector (Nx = 11) and count rate as the one-dimensional output vector (Ny = 1). In this study, about four-year data (from

February 1, 2018 to March 31, 2022) are used for machine learning. We used six-hour averaged values, i.e., a total of 9114 data points exist in the time axis.

2.2. Mass weighted temperature correction for muon count rate

The muons are created in the air shower developing in the atmosphere. The atmospheric density and temperature profiles affect the production and propagation of muons. Due to the short lifetime of muons, the muon count rate at the ground is susceptible to the distance between the production and detection points. The count rate decreases with increasing the distance due to the atmospheric expansion by the temperature increase. Therefore, applying the so-called temperature corrections to muon data is necessary before analyzing the primary cosmic ray variations.

The mass weighted (MSS) method (Mendonsa et al., 2016) first calculates the mass-weighted temperature T_{MSS} from the temperatures T_i at an atmospheric layer at altitude h_i as

$$T_{MSS} = \sum_{i=0}^{n} w(h_i) T(h_i) . \tag{6}$$

The air-mass weighted function w is defined as

$$w(h_i) = \left(x(h_i) - x(h_{i+1}) \right) / x(h_0) , \tag{7}$$

where x is the atmospheric depth in unit of (g/cm^2). In this paper we use the atmospheric pressure at h_i for $x(h_i)$ in Equation (7).

The correction based on the linear correlation between the T_{MSS} and muon count rate is the best method for muon detector data (Mendonsa et al., 2016). In this study, we applied the same MSS method to the muon detector data at Syowa Station as Kato et al. (2021) documented. To calculate the T_{MSS}, the temperature data was obtained from GDAS (Global Data Assimilation System; https://www.ncei.noaa.gov/products/weather-climate-models/global-data-assimilation) at 925, 850, 700, 600, 500, 400, 300, 250, 200, 150, 100, 70, 50, 30, and 20 hPa. Note that GDAS is different from ERA5, but we use GDAS for the temperature correction to follow the previous studies.

2.3. PARMA-based snow cover correction for neutron counting rate

The pressure correction is the major atmospheric correction necessary for the neutron count rate because the lifetime of neutrons is long, and the air-shower production dominantly depends on the air mass above the detector.

It is, however, also known that the neutron monitor count rate decreases when the accumulation of snow increases around the detector housing because of albedo neutrons scattered from the soil

moisture or the snow cover of the surrounding ground area (Schron et al., 2016; Brall et al., 2021). The snow cover effect is not negligible for the NM64-type detector used at Syowa Station because the thickness of the reflector is only 7.5 cm (c.f., 28 cm in the IGY detector), and the evaporation neutrons produced from the surrounding material can significantly contribute to the counting rate with ~5 % (Hatton, 1971). This paper discusses the snow cover effect in the polar region, while Ruffolo et al. (2016) discussed a similar "water vapor" environmental effect in the tropical region. Here, we do not anticipate the impact of the snow accumulation on the roof because the strong wind at Syowa Station tends to blow the roof snow away in a short time scale.

Japan Meteorological Agency observes the snow cover depth at Syowa Station at the Kitano-Ura area, several hundred meters away from the cosmic ray detector. The actual snow cover around the neutron monitor can be different depending on neighbor buildings and ground slopes. Also, the most significant human activity in snow removal is usually in November or December, depending on the occurrence of blizzard activities, while minor removals have been done randomly throughout the year. Therefore, to estimate the snow cover depth around the detector, we first use the observed snow cover depth between February and November and reset the estimated snow cover depth to be zero at the beginning of February each year. We then linearly interpolated the snow cover depth between November to February. Further, we put zero in the data gap of the snow cover estimation before June 2018, considering the microgravity observation at that time (Aoyama et al., 2016).

For the snow cover correction, we adopted the PARMA (PHITS-based Analytical Radiation Model in the Atmosphere) model (Sato, 2015; 2016) for calculating the neutron count rates. It can reproduce the influence of the surrounding environment on the neutron flux as a function of the underground water density (Sato and Niita, 2006). The calculated neutron fluxes were converted to the count rates, using the response function of the NM64-type detector (Sato et al. 2014). In this study, we assumed the linear relationship between the estimated snow depth, d, and the underground water density supplying to the PARMA model, q, as written by $q = c_1 + c_2 d$, where c_1 and c_2 are the constant parameters. We fixed the numerical value of c_1 to be 0.20, commonly used for calculating the neutron monitor count rate (Sato 2015). On the other hand, we regarded c_2 as a free parameter determined to minimize the χ^2 value between the calculated and measured count rates. We can estimate the snow correction factor from the ratio between neutron count rates calculated by PARMA with and without the snow cover effect (**Appendix C**).

Figure 2 shows the estimated snow cover depth, the pressure-corrected relative count rates of the neutron monitor obtained from the observation, and the results of PARMA with different c_2 parameters. The relative count rates are normalized to their mean value in February 2019, when there was little

snow around the neutron monitor. It is apparent from the figure that the measured count rates are anti-correlated with the snow cover depth. The best-fit value of c_2 to the observation is 0.45 m^{-1}, with the maximum coefficient of determination $R^2 = 0.69$.

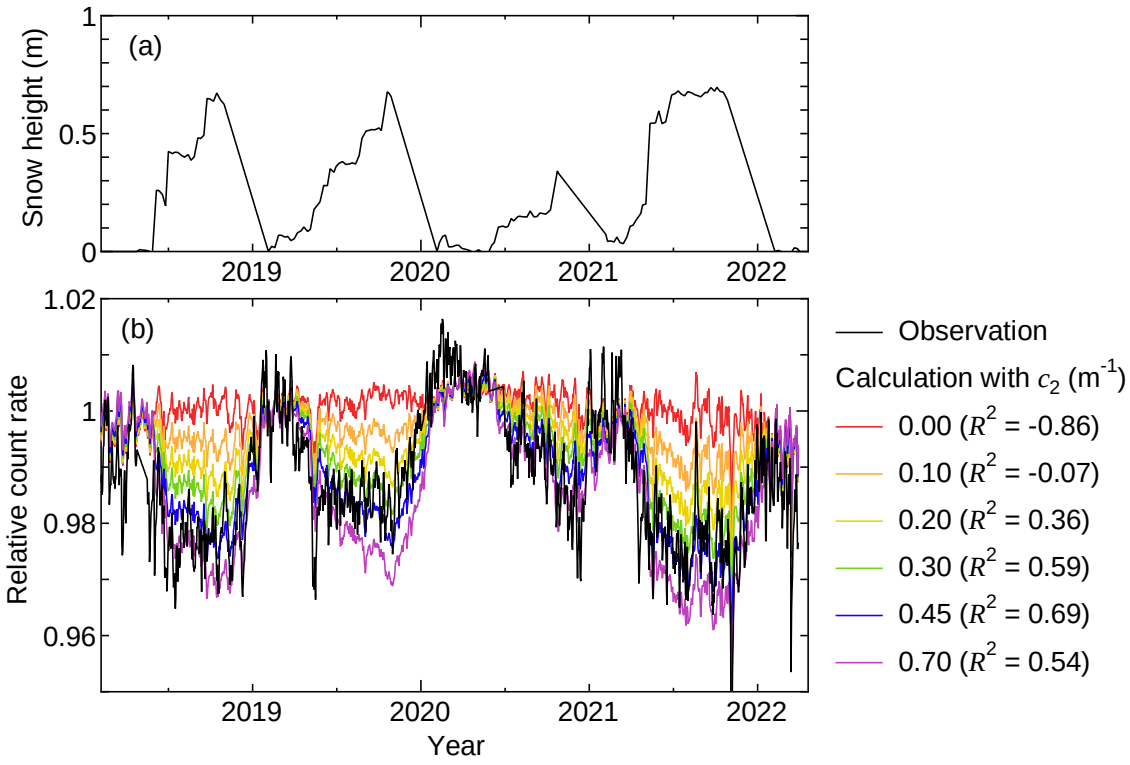

Figure 2. Estimated snow cover depth (top panel) and the pressure-corrected relative count rates of the neutron monitor as obtained from the observation and the PARMA calculation with different c_2 parameters (bottom panel).

3. Comparison among different correction methods

We compare the MSS and ESN temperature correction on the muon count rate (**Figure 3**). **Figure 3b** shows the temperature effects on the muon count rate reproduced by the two methods. Note that a data gap in muon count rate existed at the beginning of 2021. **Figure 3c** shows the corrected count rates estimated from the ESN and MSS methods. Similar decreasing trends of ~2% per year appeared in 2020 and continued in 2021 in **Figure 3c**. The seasonal variation remains in the MSS corrected count rate, and the most notable difference between MSS and ESN appears around the end of each year. The difference between MSS and ESN results makes it challenging to identify the exact start timing of the decreasing trend, but it is safe to say that it roughly corresponds to the solar minimum in late 2019.

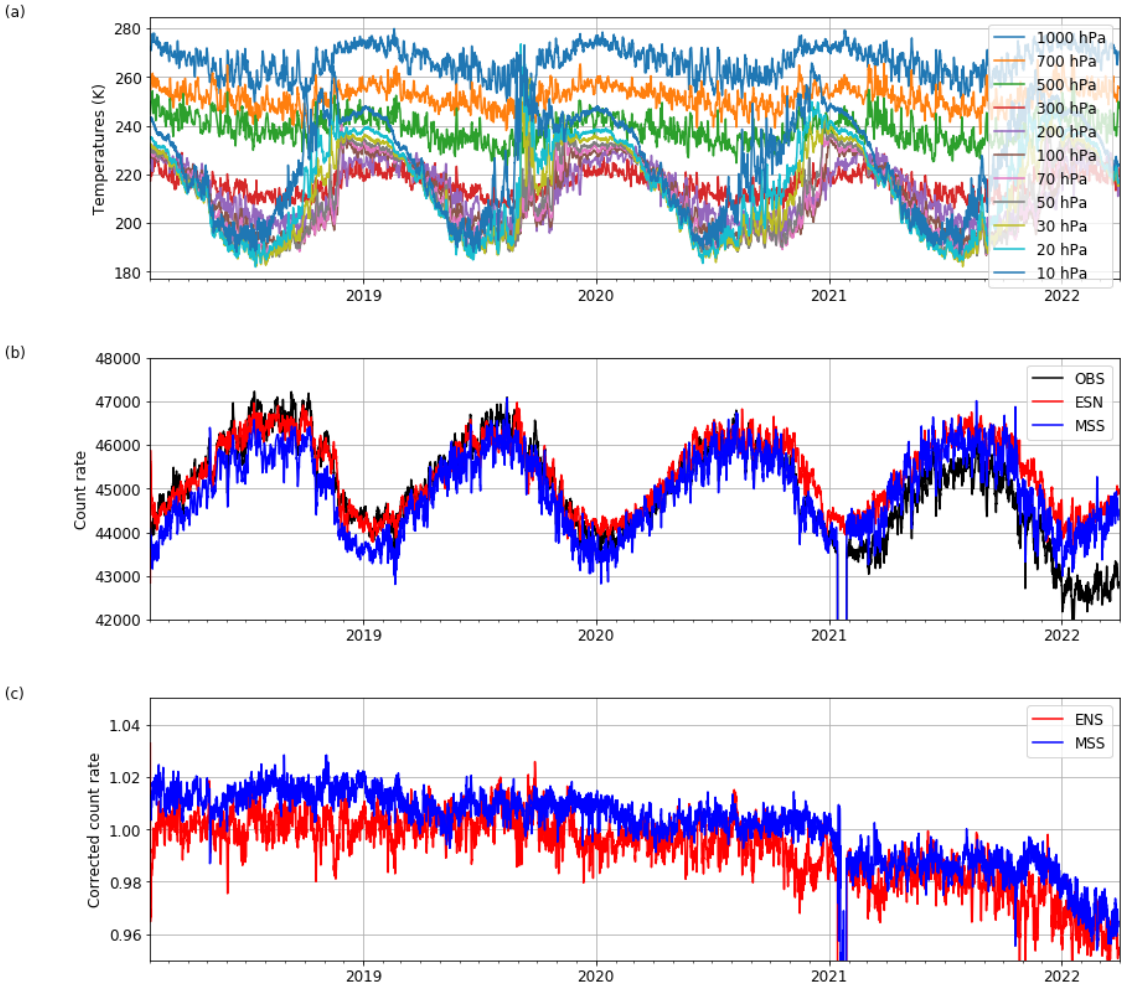

Figure 3. Data-model comparison at Syowa Station. (a) Temperatures at 1000, 700, 500, 300, 200, 100, 70, 50, 30, 20, and 10 hPa, (b) muon count rate in the unit of counts/min, (c) corrected count rate.

For the snow cover correction of the neutron counts at Syowa Station the same ESN method may also work for the neutron monitor at Syowa Station, because the time variation of the atmospheric

parameters may control the resultant snow cover around the neutron monitor. However, the chain of physics and related human activities of snow removal is very complex.

Figure 4 shows the snow cover corrections applied to the neutron count rate at Syowa Station, using the PARMA and ESN models. The snow cover effects reproduced by two methods are shown in Figure 4b, while Figure 4c shows the corrected count rates (**Appendix C**). It is apparent that both methods similarly removes the seasonal variation due to the snow cover. In **Figure 4c**, a negative spike in May 2019 is a natural variation associated with multiple CMEs passing across the Earth. Similar Forbush decrease events associated with CMEs can also be identified in November 2021 and March 2022. However, the large bipolar variation in December 2020 is associated with the human activity of snow removal, which is not a natural variation of primary cosmic rays. Note also that the solar activity was relatively quiet in December 2020.

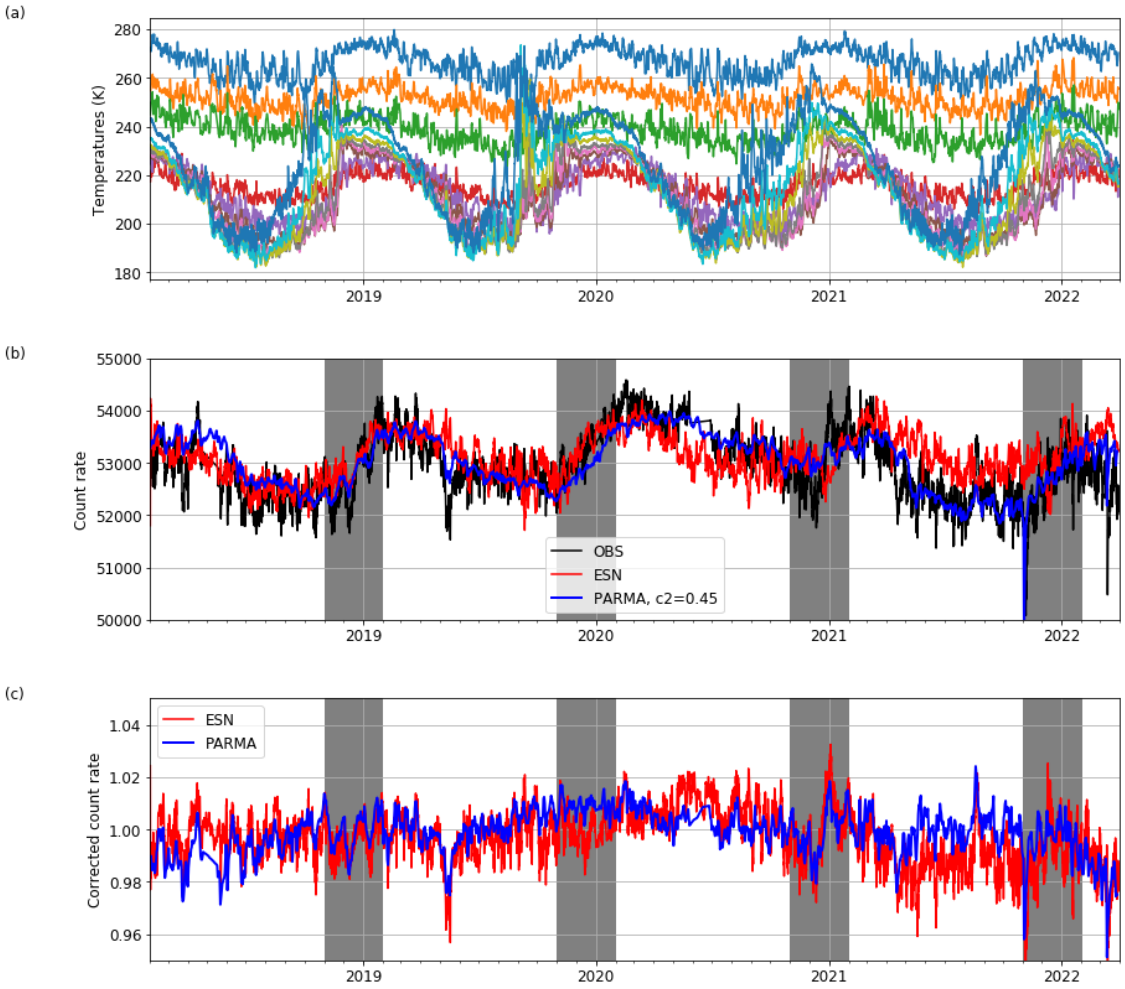

Figure 4. Data-model comparison at Syowa Station. (a) Temperatures at 1000, 700, 500, 300, 200, 100, 70, 50, 30, 20, and 10 hPa, (b) neutron count rate in the unit of counts/min, (c) corrected count

rate.

The decreasing trend starts in the somewhere early half of 2020 in both PARMA and ESN results, which is roughly consistent with Oulu neutron monitor data (**Figure 1**). Careful analysis using multiple stations is also needed to estimate the possible lag between muon count rate and neutron count rate. We must monitor the actual snow cover situation around the neutron monitor in future observations for further detailed snow cover correction.

Note that the ESN-based correction of the snow-cover effect on the neutron count rate has a complex meaning. First, the input temperature data of ERA5 correlates with the snow cover, which can also be confirmed by the ESN method (**Appendix D**). Second, snow-drift accumulation effects, blizzard occurrence, and artificial snow removal activities are also related to the temperature data. The ESN learned the whole correlations among all of these natural and artificial effects.

The decreasing trend started earlier in the muon detector around the solar minimum in late 2019, while it started several months later in the neutron monitor in early 2020. We can theoretically interpret the possible lag as follows. Protons with energies of 5 GeV and 25 GeV, for example, move in the similar speed (98.2% and 99.9% of the speed of light, respectively), but the gyro radii are 0.1 AU and 0.5 AU for ~1 nT magnetic field, respectively. Due to gyro motions with different gyro radii, the propagation time of low-energy particles tends to be longer than that of high-energy particles. Also, high-energy particles can come close to the Sun earlier and get sensitively affected by the changing solar magnetic field. As a result, low-energy particles show a delayed and smoothed solar modulation profile compared to high-energy particles. Therefore, the earlier response of the muon count rate around the sunspot minimum is qualitatively consistent with the existing theories. Therefore, the possible lag of a few to several months are also within expectation.

Note also that the time lag of low-energy cosmic ray variation to higher energy has been discussed as the “hysteresis effect” of the solar modulation (Moraal, 1976). We can model the hysteresis effect by considering the rigidity-dependent component of the diffusion coefficient, using the force-field approximation of the steady-state spherically symmetric modulation equations. O’Gallagher (1975) proposed a time-dependent diffusion-convection model to interpret the observed time delay of low-energy particles.

By analyzing the long-term variations of neutron and muon count rates, Nagashima and Morishita (1980) reported that the lag is systematically longer in odd solar activity cycles, including $A>0$ to $A<0$ transition of the solar polar magnetic field polarity than in even cycles including $A<0$ to $A>0$

transitions. The present paper documented an example only in A>0 solar minimum. We have to examine the modulation in the A<0 period and in different solar activity phases to investigate the energy-dependent solar modulation in more detail. As future work, we can better address the hysteresis effects and the energy-dependent solar modulation by carefully applying similar correction methods as developed in this study to long-term data of both neutron monitors and muon detectors.

4. Conclusions

We proposed a new snow cover correction method for the neutron count rate using the PARMA model. We then showed that the ESN model combined with the ERA5 temperature time series could be useful for the snow cover correction of neutrons and the temperature correction for muons, showing the reasonable agreement among different correction methods. From the comparisons of the corrected count rates, we conclude that muons likely started to decrease at least a few months earlier (late 2019) than neutrons (early 2020), which can be interpreted by a standard understanding of the energy-dependent intrusion of cosmic ray protons.

Acknowledgments:

RK thanks Okinawa Institute of Science and Technology for hosting his sabbatical visit. RK thanks Gen Hashida, Shuki Ushio, Yuichi Aoyama, and Akihisa Hattori, in their advice for using the snow cover data at Syowa Station. We acknowledge the use of ERA5 and GDAS reanalysis data. The polar magnetic field data is obtained from WSO. Sunspot number is obtained from SILSO ver 2.0. We thank the use of Oulu neutron monitor data.

References:

Aoyama, Y., K. Doi, H. Ikeda, H. Hayakawa, and K. Shibuya (2016), Five years' gravity observation with the superconducting gravimeter OSG#058 at Syowa Station, East Antarctica: gravitational effects of accumulated snow mass, Geophysical Journal International, Volume 205, Issue 2, 1290-1304, https://doi.org/10.1093/gji/ggw078

Brall, T., V. Mares, R. Butikofer, and W. Ruhm (2021), Assessment of neutrons from secondary cosmic rays at mountain altitudes – Geant4 simulations of environmental parameters including soil moisture and snow cover, The Cryosphere.

Butikofer, R. (2018). Ground-Based Measurements of Energetic Particles by Neutron Monitors. In: Malandraki, O., Crosby, N. (eds) Solar Particle Radiation Storms Forecasting and Analysis. Astrophysics and Space Science Library, vol 444. Springer, Cham.

Hatton, C. J. (1971), The Neutron Monitor, Prog. Elem. Part. Cosmic Ray Phys., Ed. Wilson and Wouthuysen, Vol. 10.

Hersbach, H., Bell, B., Berrisford, P., Biavati, G., Horanyi, A., Munoz Sabater, J., Nicolas, J., Peubey,

C., Radu, R., Rozum, I., Schepers, D., Simmons, A., Soci, C., Dee, D., Thepaut, J-N. (2018): ERA5 hourly data on pressure levels from 1979 to present. Copernicus Climate Change Service (C3S) Climate Data Store (CDS). (Accessed on 28-NOV-2021), https://doi.org/10.24381/cds.bd0915c6

Hersbach, H., Bell, B., Berrisford, P., Hirahara, S., Horanyi, A., Munoz-Sabater, J., et al. (2020). The ERA5 global reanalysis. Quarterly Journal of the Royal Meteorological Society, 146(730), 1999-2049. https://doi.org/10.1002/qj.3803

Jaeger, H. (2001). The "echo state" approach to analysing and training recurrent neural networks, GMD Report 148. GMD - German National Research Institute for Computer Science.

Kataoka, R., T. Sato, Y. Kubo, D. Shiota, T. Kuwabara, S. Yashiro, and H. Yasuda (2014), Radiation dose forecast of WASAVIES during ground level enhancement, Space Weather, 12, doi:10.1002/2014SW001053.

Kataoka, R., T. Sato, S. Miyake, D. Shiota, and Y. Kubo (2018), Radiation Dose Nowcast for the Ground Level Enhancement on 10-11 September 2017, Space Weather, 16, https://doi.org/10.1029/2018SW001874.

Kataoka, R., and S. Nakano (2021), Reconstructing solar wind profiles associated with extreme magnetic storms: A machine learning approach, Geophysical Research Letters, 48, e2021GL096275. https://doi.org/10.1029/2021GL096275.

Kato, C., W. Kihara, Y. Ko, A. Kadokura, R. Kataoka, P. Evenson, S. Uchida, S. Kaimi, Y. Nakamura, H. A. Uchida, K. Murase, and K. Munakata (2021), New cosmic ray observations at Syowa Station in the Antarctic for space weather study, J. Space Weather Space Clim., 11, 31.

Kihara W., C. Braga, R. Mendonca, A. Lago, N. Schuch, M. Rockenbach, E. Echer, J. Bageston, M. Duldig, J. Humble, P. Evenson, J. Kota, M. M. Sharma, H. AlJassar, I. Sabbah, K. Munakata, C. Kato, M. Kozai, T. Kuwabara, R. Kataoka, A. Kadokura, S. Miyake, and M. Tokumaru (2021), A Peculiar ICME Event in August 2018 Observed with the Global Muon Detector Network, Space Weather, 19, e2020SW002531. https://doi.org/10.1029/2020SW002531.

Mendonsa, R. et al. (2016), The temperature effect in secondary cosmic rays (MUONS) observed at the ground: analysis of the global muon detector network data, Astrophys. J., 830(2), 88-112.

Miyake, S., R. Kataoka, and T. Sato (2017), Cosmic ray modulation and radiation dose of aircrews during the solar cycle 24/25, Space Weather, 15(4), 589-605, doi:0.1002/2016SW001588.

Moraal, H. (1976), Observations of the eleven-year cosmic-ray modulation cycle, Space Science Reviews, 19, 845-920.

Murakami, K., Nagashima, K., Sagisaka, S. et al. (1979), Response functions for cosmic-ray muons at various depths underground. Il Nuovo Cimento C 2, 635-651. https://doi.org/10.1007/BF02557762

Nagashima, K. and Morishita, I. (1980), Twenty-two year modulation of galactic cosmic rays

associated with polarity reversal of polar magnetic field of the sun, Planet Space Sci., 28 195-25. https://doi.org/10.1016/0032-0633(80)90095-1

Nagashima, K., Sakakibara, S., Murakami, K. et al. (1989), Response and yield functions of neutron monitor, galactic cosmic-ray spectrum and its solar modulation, derived from all the available world-wide surveys. Il Nuovo Cimento C 12, 173-209. https://doi.org/10.1007/BF02523790

O'Gallagher, J. J. (1975), A time-dependent diffusion-convection model for the long-term modulation of cosmic rays, The Astrophysical Journal, 197, 495-507.

Ruffolo, D., et al. (2016), MONITORING SHORT-TERM COSMIC-RAY SPECTRAL VARIATIONS USING NEUTRON MONITOR TIME-DELAY MEASUREMENTS, ApJ, 816, 38.

Sato, T. and K. Niita (2006), Analytical Function to Predict Cosmic-Ray Neutron Spectrum in the Atmosphere, Radiat. Res. 166, 544-555.

Sato, T., R. Kataoka, H. Yasuda, Y. Seiji, T. Kuwabara, D. Shiota, and Y. Kubo (2014), Air shower simulation for WASAVIES: Warning system for aviation exposure to solar energetic particles, Radiation Protection Dosimetry, 161, doi:10.1093/rpd/nct332.

Sato, T, R. Kataoka, D. Shiota, Y. Kubo, M. Ishii, H. Yasuda, S. Miyake, I. Park, and Y. Miyoshi (2018), Real-Time and Automatic Analysis Program for WASAVIES: Warning System of Aviation Exposure to Solar Energetic Particles, Space Weather, 16, https://doi.org/10.1029/2018SW001873.

Sato, T. (2015), Analytical Model for Estimating Terrestrial Cosmic Ray Fluxes Nearly Anytime and Anywhere in the World: Extension of PARMA/EXPACS, PLOS ONE 10(12): e0144679 DOI: 10.1371/journal.pone.0144679

Sato, T. (2016), Analytical Model for Estimating the Zenith Angle Dependence of Terrestrial Cosmic Ray Fluxes. PLOS ONE 11(8): e0160390 (2016). DOI: 10.1371/journal.pone.0160390

Schron, M., S. Zacharias, M. Kohli, J. Weimar and P. Dietrich (2016), Monitoring Environmental Water with Ground Albedo Neutrons from Cosmic Rays, Volume 236 - The 34th International Cosmic Ray Conference (ICRC2015) - Cosmic Ray Physics: Methods, Techniques and Instrumentation, Published on: August 18, 2016, DOI: https://doi.org/10.22323/1.236.0231

Appendix:

A: Response function and primary median energy

We calculate the response function for the Syowa neutron monitor using the method given by Nagashima et al. (1989). For the muon detector, for the vertical incident direction, we used the interpolation values from the table of the response function calculated by Murakami et al. (1979). We define the median primary rigidities as the rigidity at which the normalized integral response function equals 0.5.

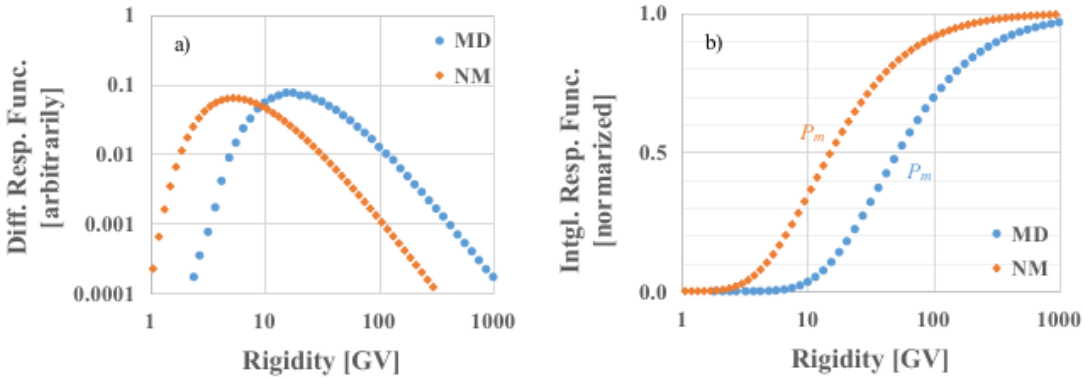

Figure A1: a) Differential and b) integral response functions of the muon detector (solid blue circle) and neutron monitor (solid orange diamond) at Syowa Station. Differential response functions are leveled, while the integral response functions are normalized.

B: Hyperparameter survey for echo-state network

Root mean square error between the observation and model decreases as the spectral radius is greater for both muon modeling (left panel of Figure B1) and neutron modeling (right panel of Figure B1). To guarantee the echo state property, we selected the spectral radius of 0.95 (below unity).

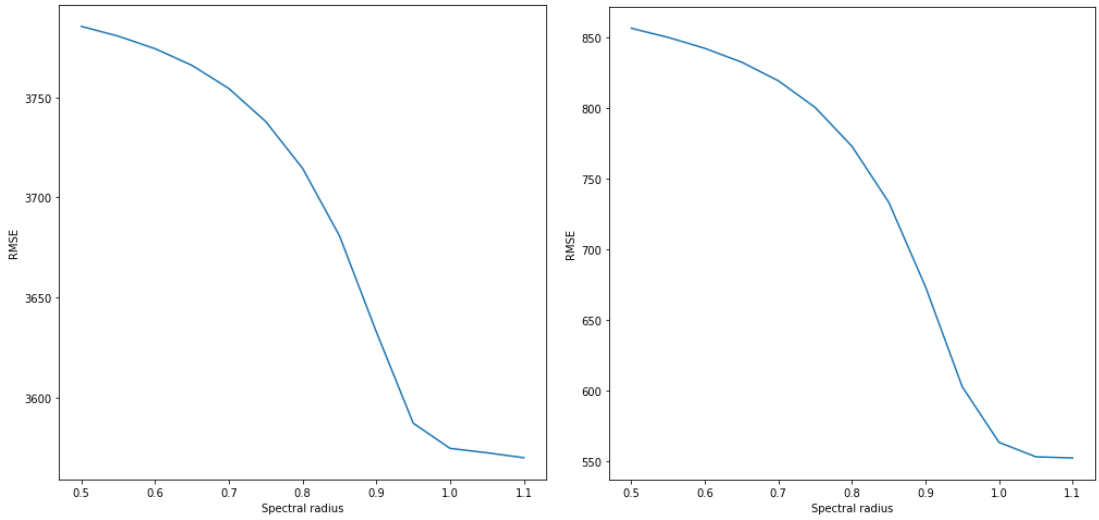

Figure B1: Root mean square errors between observed and modeled muon count rate (left) and neutron count rate (right), changing the spectral radius of the echo state network. We set the number of nodes to be 10^3.

C. Corrected count rate and correction factor

The corrected count rate I_{corr} and correction factor A_{corr} can be defined as follows:

$$I_{\text{corr}} = I_{\text{obs}} A_{\text{corr}},$$

$$A_{\text{corr}} = \frac{I_{\text{base}}}{I_{\text{actual}}},$$

where I_{obs} is the observed count rate, I_{base} and I_{actual} are the model-estimated count rates for the base and actual conditions, respectively. For the snow cover correction using PARMA, I_{base} and I_{actual} were calculated by setting q = 0.2 and 0.2 + 0.45d, respectively. As another example, for the standard pressure correction of neutron count rate, A_{corr} can be described as follows:

$$A_{corr} = \exp\left(-R_{\text{model}}\right),$$

$$R_{\text{model}} = \ln\left(\frac{I_{\text{actual}}}{I_{\text{base}}}\right) = \frac{\beta}{100}\Delta P,$$

where ΔP is the difference between the actual and base pressures, and β is the correlation coefficient in the unit of [%/hPa].

D. Example of the ESN model to reproduce the snow cover

To test the ability of the ESN model to reproduce the snow cover, we replace the output vector of the ESN model with the estimated snow cover data. The input data is the same ERA5 temperature time series used in the main contents. The basic seasonal variation of the estimated snow cover is reasonably

reproduced, although the disagreement is considerable in 2021.

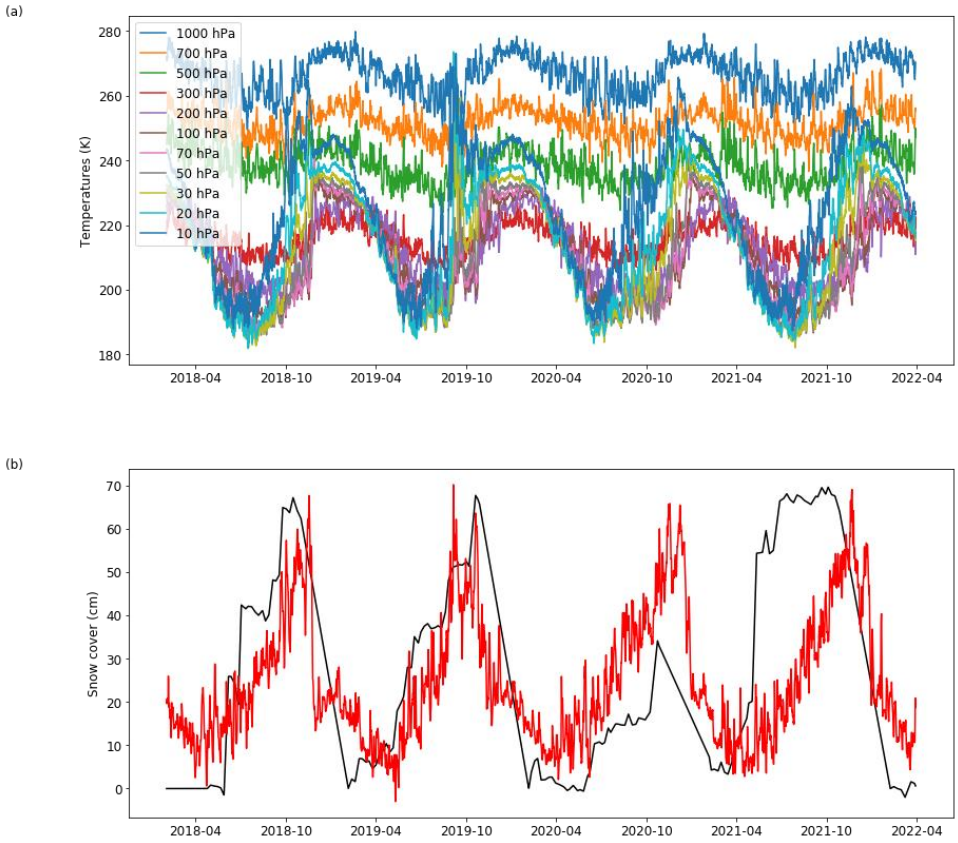

Figure D1. (a) Input vectors of ERA5 temperatures at 1000, 700, 500, 300, 200, 100, 70, 50, 30, 20, and 10 hPa and (b) output vector of the snow cover depth with the ESN result (red).